Inorg. Chem. **2008**, *47*, 8336−8342

Hybrid Organic−Inorganic Framework Structures: Influence of Cation Size on Metal−Oxygen−Metal Connectivity in the Alkaline Earth Thiazolothiazoledicarboxylates

Eduardo H. L. Falcão,[†] Naraso,[‡] Russell K. Feller,[†,‡] Guang Wu,[‡] Fred Wudl,[‡] and Anthony K. Cheetham*[,†,§]

Materials Research Laboratory, University of California, Santa Barbara, California 93106, Department of Chemistry and Biochemistry, University of California, Santa Barbara, California 93106, and Department of Materials Science and Metallurgy, University of Cambridge, Pembroke Street, Cambridge CB2 3QZ, United Kingdom

Received May 19, 2008

We report the synthesis of four organic−inorganic frameworks of alkaline earth cations with the organic ligand 2,5-thiazolo[5,4-*d*]thiazoledicarboxylate ($C_6N_2S_2O_4^{2-}$, Thz^{2-}). Structures with remarkably different connectivities result when Mg^{2+}, Ca^{2+}, Sr^{2+}, and Ba^{2+} react with Thz^{2-}. $Mg(Thz)(H_2O)_4$ (**I**) forms a 1-D coordination polymer in which one carboxylate oxygen on each terminus of the ligand connects individual MgO_6 octahedra from their axial positions, while the remaining equatorial sites are coordinated by water molecules. $Ca_2(Thz)_2(H_2O)_8$ (**II**) forms a 1-D coordination polymer in which dimeric clusters with 7-fold Ca coordination are connected via the ligand in a linear fashion, with a second, uncoordinated Thz^{2-} providing charge balance. $Sr(Thz)(H_2O)_3$ (**III**) has 1-D infinite inorganic connectivity built from edge-sharing SrO_7N polyhedra having one carboxylate oxygen and one water molecule acting as M−O−M bridges. $Ba_2(Thz)_2(H_2O)_7$ (**IV**) has 2-D inorganic connectivity based upon face- and edge-sharing BaO_9N polyhedra. One carboxylate oxygen and all water molecules act as bridges between each Ba^{2+} and its three neighbors. We shall discuss the manner in which the increasing coordination requirements of the cations (MgO_6 < CaO_7 < SrO_7N < BaO_9N) lead to an increase in inorganic connectivity through the series.

Introduction

There has been a growth of interest in hybrid organic−inorganic structures during the past decade, partly driven by their emerging applications in areas such as catalysis, ion exchange, and gas storage.[1−8] While these uses typically involve porous frameworks, denser structures are now attracting considerable attention on account of their magnetic, optical, and electronic properties.[9,10] The structural and chemical diversity of hybrid systems is immense,[11] and it has become important to try to better understand the factors that influence this diversity of behavior. A wide range of factors is clearly important, for example, the identity of the cation, the nature of the ligand, the reaction temperature, and the solvent, but significant progress has been made in this area. Template effects have also received growing interest for pore and architectural tuning.[8] Most hybrid framework materials are synthesized from solution, often under hydrothermal or solvothermal conditions, and we have shown that increasing the reaction temperature and pH leads to structures with higher dimensionalities and lower levels of hydration.[12,13] The trend with increasing temperatures may

* Author to whom correspondence should be addressed. Phone: 01223-767061. E-mail: akc30@cam.ac.uk.
[†] Materials Research Laboratory, University of California.
[‡] Department of Chemistry and Biochemistry, University of California.
[§] University of Cambridge.

(1) Kitagawa, S.; Kitaura, R.; Noro, S. *Angew. Chem., Int. Ed.* **2004**, *43*, 2334.
(2) Férey, G. *Chem. Soc. Rev.* **2008**, *37*, 191.
(3) Shvareva, T. Y.; Skanthakumar, S.; Soderholm, L.; Clearfield, A.; Albrecht-Schmitt, T. E. *Chem. Mater.* **2007**, *19*, 132.
(4) Rowsell, J. L. C.; Yaghi, O. M. *Angew. Chem., Int. Ed.* **2005**, *44*, 4670.
(5) Rosseinsky, M. J. *Microporous Mesoporous Mater.* **2004**, *73*, 15.
(6) Rao, C. N. R.; Natarajan, S.; Vaidhyanathan, R. *Angew. Chem., Int. Ed.* **2004**, *43*, 1466.
(7) Morris, R. E.; Wheatley, P. S. *Angew. Chem., Int. Ed.* **2008**, *47*, 4966.
(8) Tanaka, D.; Kitagawa, S. *Chem. Mater.* **2008**, *20*, 922.
(9) Cheetham, A. K.; Rao, C. N. R. *Science* **2007**, *318*, 58.
(10) Rao, C. N. R.; Cheetham, A. K.; Thirumurugan, R. *J. Phys. Condens. Matter* **2008**, *20*, 083202.
(11) Cheetham, A. K.; Rao, C. N. R.; Feller, R. K. *Chem. Commun.* **2006**, *4780*.

10.1021/ic8009173 CCC: $40.75
Published on Web 08/20/2008

Chart 1

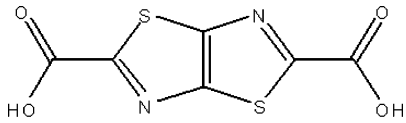

H_2Thz

be reflected in terms of forming coordination polymers with higher dimensionalities (e.g., $I^0O^0 \rightarrow I^0O^1 \rightarrow I^0O^2 \rightarrow I^0O^3$ according to the classification in ref 11), by increasing the inorganic connectivity (e.g., $I^0O^1 \rightarrow I^1O^1 \rightarrow I^2O^1 \rightarrow I^3O^1$), or by combinations of these effects. We have also shown that the use of flexible ligands is more likely to give rise to extended inorganic connectivity[14] and that chiral ligands can give rise to structures with higher dimensionalities.[15] There is considerable evidence that thermodynamic control is very important in such situations, though differing results from the use of conventional and microwave heating point to kinetic control under some circumstances.[16,17]

Turning to the work of other groups who have focused on such questions, a series of lead dicarboxylate frameworks was investigated by Yang et al.[18] The nature of the organic dicarboxylic acid, the coligand, and the solvent determined whether 1-D, 2-D, or 3-D structures would form, and supramolecular interactions such as $\pi-\pi$ stacking also played a role in determining the crystal structure of some of the compounds. In work by Duan et al.[19] on a series of alkaline earth methylenediisophthlate hybrid frameworks, reactions with magnesium result in 1-D chiral chains, while Ca, Sr, and Ba form 2-D layered structures, with Sr and Ba showing very similar M−O−M motifs. Clear evidence that cation size can be very important is found in the recent work by Côté and Shimizu[20] on a series of alkaline earth organosulfonates; all but one of the structures are coordination polymers, and their dimensionalities progress from 0-D through 1-D and 2-D to 3-D with Mg, Ca, Sr, and Ba, respectively.

In the present work, we utilize 2,5-thiazolo[5,4-*d*]thiazoledicarboxylic acid (H_2Thz, see Chart 1) to form hybrid organic−inorganic frameworks with the alkaline earths Mg, Ca, Sr, and Ba. This ligand is interesting in that it features not only the two carboxylate groups but also nitrogen and sulfur heteroatoms within the rigid linker, potentially offering additional binding sites and more structural flexibility in the formation of the frameworks. The resulting frameworks show how increasing the cation size and coordination requirements lead to greater inorganic connectivity in this system. Namely, the dimensionality (as defined in ref 11) progresses from I^0O^1 to I^0O^1 to I^1O^0 to I^2O^0 as one goes down the group.

Experimental Section

The synthesis of H_2Thz was adapted from the published reaction.[21] The detailed procedure is available as Supporting Information. All other reagents were used as purchased. Solutions were prepared in deionized water and commercial 99+% pyridine (Aldrich) and were flushed with a stream of nitrogen for a few minutes before closing the reaction vessel. Identical hydrothermal conditions were used for the synthesis of the frameworks with magnesium, calcium, and strontium.

In general, 0.1 mmol of the alkaline earth acetate and 0.05−0.06 mmol of H_2Thz (12 mg) were dissolved in a mixture consisting of 5 mL of water and 4 mL of pyridine. Teflon-lined Parr autoclaves or thick-walled glass reaction tubes (capacities 22 and 15 mL, respectively) were used as reaction vessels; the reaction temperature and time were 100 °C and ∼24 h, respectively. The resulting colorless crystals were filtered, rinsed with water and acetone, and dried in the air at ∼60 °C for 5−10 min.

The formation of $Mg(Thz)(H_2O)_4$ (**I**) and $Sr(Thz)(H_2O)_3$ (**III**) under hydrothermal conditions was very facile and reproducible. Even after a few hours of reaction, small colorless crystals could be seen on the walls of the glass reactors in both cases. Crystals of $Ca_2(Thz)_2(H_2O)_8$ (**II**) were easily obtained from the reaction between $Ca(CH_3CO_2)_2$ and H_2Thz, but their quality depended heavily on the experimental conditions; good-quality crystals required a very stable, vibration-free oven and slow, undisturbed cooling. Typical yields were 20% (**I**), 37% (**II**), and 65% (**III**).

For the synthesis of $Ba_2(Thz)_2(H_2O)_7$ (**IV**), slow crystallization from an open, hot solution was accomplished according to the following procedure: ∼23 mg of H_2Thz was dissolved in a warm (typically 60−100 °C) water/pyridine mixture (approximately 30 and 10 mL, respectively). A total of 51 mg of $Ba(CH_3CO_2)_2$ was dissolved in a second water/pyridine mixture (∼15 and 5 mL, respectively). This second solution was slowly added to the hot H_2Thz solution. Normally, no immediate precipitation would be observed, but as the solvents evaporated, crystals formed. The addition of more $Ba(CH_3CO_2)_2$ would cause precipitation of lower-quality crystals, and rapid mixing of more concentrated solutions produced white powders. The powder X-ray diffraction (XRD) patterns of these products, however, always matched the simulated pattern of **IV** or the powder pattern of its ground crystals. The reaction was reproducible up to temperatures close to 100 °C. After filtration and drying, ∼12 mg of white crystals were collected. Yield was ∼28% on the basis of the crystallographic formula, although much higher yields (60−75%) were attainable if the crystal quality was unimportant.

Elemental analysis results were as follows (percents calculated from formulas are in parentheses). **I**: C, 22.3% (22.20); H, 2.2% (2.48); N, 8.2% (8.63). **II**: C, 21.4% (21.17); H, 2.0% (2.37); N, 8.2% (8.23). **III**: C, 18.4% (19.48); H, 1.6% (1.63); N, 6.9% (7.58). **IV**: C, 17.9% (16.81); H, 1.4% (1.65); N, 6.4% (6.54).

Suitable single crystals were selected under a polarizing microscope and glued to glass fibers. Intensity data were collected at room temperature on a Siemens SMART CCD diffractometer (Mo Kα radiation, $\lambda = 0.71073$ Å). The structures were solved using direct methods and difference Fourier synthesis. Refinement details are reported as Supporting Information.

(12) Forster, P. M.; Burbank, A. R.; Livage, C.; Férey, G.; Cheetham, A. K. *Chem. Commun.* **2004**, *368*.
(13) Forster, P. M.; Stock, N.; Cheetham, A. K. *Angew. Chem., Int. Ed.* **2005**, *44*, 7608.
(14) Forster, P. M.; Cheetham, A. K. *Microporous Mesoporous Mater.* **2004**, *73*, 57.
(15) Kam, K. C.; Young, K. L. M.; Cheetham, A. K. *Cryst. Growth Des.* **2007**, *7*, 1522.
(16) Jhung, S. H.; Lee, J.-H.; Forster, P. M.; Férey, G.; Cheetham, A. K.; Chang, J.-S. *Chem.—Eur. J.* **2006**, *12*, 7899.
(17) Jhung, S. H.; Lee, J.-H.; Yoon, J. W.; Serre, C.; Férey, G.; Chang, J.-S. *Adv. Mater.* **2007**, *19*, 121.
(18) Yang, J.; Li, G.-D.; Cao, J.-J.; Yue, Q.; Li, G.-H.; Chen, J.-S. *Chem.—Eur. J.* **2007**, *13*, 3248.
(19) Duan, X.; Lin, J.; Li, Y.; Zhu, C.; Meng, Q. *CrystEngComm* **2008**, *10*, 207.
(20) Côté, A. P.; Shimizu, G. K. H. *Chem.—Eur. J.* **2003**, *9*, 5361.
(21) Johnson, J. R.; Rotenberg, D. H.; Ketcham, R. *J. Am. Chem. Soc.* **1970**, *92*, 4046.

Table 1. Crystallographic Data and Structure Refinement Parameters[a]

compound	I. $Mg(Thz)(H_2O)_4$	II. $Ca(Thz)(H_2O)_4$	III. $Sr(Thz)(H_2O)_3$	IV. $Ba_2(Thz)_2(H_2O)_7$
chemical formula	$MgC_6H_8O_8N_2S_2$	$CaC_6H_8O_8N_2S_2$	$SrC_6H_6O_7N_2S_2$	$Ba_2C_{12}H_{14}O_{15}N_4S_4$
fw	324.57	340.34	369.87	857.19
temp. (K)	293	298	298	298
cryst syst	triclinic	triclinic	monoclinic	monoclinic
space group	$P\bar{1}$	$P\bar{1}$	$P2_1/c$	$C2/c$
a/Å	5.032 (5)	7.182 (4)	7.1852 (6)	13.2701 (13)
b/Å	7.426 (8)	7.989 (4)	23.6079 (18)	7.9050 (8)
c/Å	7.877 (9)	11.573 (6)	6.8973 (5)	22.428 (2)
α/deg	85.27 (2)	92.448 (9)	90	90
β/deg	85.17 (2)	101.235 (9)	95.973 (2)	98.773 (3)
γ/deg	73.33 (2)	112.596 (8)	90	90
cell vol./Å^3	280.5 (5)	596.2 (5)	1163.62 (16)	2325.2 (4)
Z	1	2	4	4
ρ (calc.) (g/cm^3)	1.922	1.896	2.111	2.449
μ (mm^{-1})	0.571	0.915	5.020	3.809
F_{000}	166	348	728	1640
cryst size (mm)	0.08 × 0.02 × 0.02	0.10 × 0.01 × 0.01	0.4 × 0.1 × 0.08	0.08 × 0.06 × 0.06
θ range	2.60−26.10°	2.79−26.02°	1.73−26.64°	1.84−26.54°
reflns collected	2308	4340	9338	9085
ind. reflns	1062	2247	2345	2316
R_{int}	0.1042	0.0404	0.0332	0.0549
completeness	95.8%	95.5%	96.0%	95.9%
abs. correction	SADABS	SADABS	SADABS	SADABS
no. of parameters	101	197	183	190
GOF on $\|F\|^2$	0.994	1.023	1.084	1.086
R_1; wR_2 [$I > 2\sigma(I)$]	0.0709; 0.1306	0.0636; 0.1470	0.0346; 0.0723	0.0455; 0.0973
R_1; wR_2 [all reflections]	0.1765; 0.1773	0.1129; 0.1787	0.0469; 0.0762	0.0683; 0.1061
largest diff. peak and hole (e Å^{-3})	0.504 and −0.458	0.929 and −0.513	0.845 and −0.361	1.765 and −0.623

[a] Please refer to the Supporting Information for a list of selected bond distances and angles.

CCDC deposition numbers were 685812 for **I**, 685813 for **II**, 685814 for **III**, and 685815 for **IV** (these data can be obtained free of charge from The Cambridge Crystallographic Data Centre via www.ccdc.cam.ac.uk/data_request/cif, or by e-mailing data_request@ccdc.cam.ac.uk). See Table 1 for crystal data and structure refinement parameters.

Powder X-ray diffraction data were acquired on a Phillips X'PERT diffractometer with Cu Kα radiation (λ = 1.5418 Å). In general, 2θ ranged from 5 to 75°, and a 0.0167° step size and 5 s/step counting time were used. These XRD patterns were compared with simulated patterns based on the single crystal structures. Thermogravimetric analysis was performed with a TA Q50 TGA instrument under nitrogen. The amount of sample used for each measurement ranged from 1 to 10 mg, and the heating rates were 5 or 10 °C/min. The Supporting Information includes both the powder XRD and thermogravimetric analysis (TGA) results.

Results and Discussion

We shall first describe the individual phases, **I**−**IV**, and then discuss the trends through the series. Table 1 summarizes the structure refinement parameters and results.

$Mg(Thz)(H_2O)_4$, I. Compound **I** is a 1-D coordination polymer which crystallizes in the space group $P\bar{1}$. Four water oxygen atoms occupy equatorial positions, and two carboxylate oxygen atoms occupy axial positions on a MgO_6 octahedron, as shown in Figure 1. The metal ion lies on an inversion center; hence, only three oxygen atoms are unique: O1 from the carboxylate groups and O3 and O4 from the water molecules. The O−Mg−O angles within the equatorial plane are 91.3(2)° and 88.7(2)°; the equatorial bond distances are 2.030(6) Å (Mg−O3) and 2.027(5) Å (Mg−O4), and the axial bond distance (Mg−O1) is 2.171(6) Å. The plane defined by the fused heterocyclic ring system of the Thz unit is rotated by approximately 21° relative to the $Mg(H_2O)_4$ equatorial plane. The water hydrogen atoms deviate only slightly from this equatorial plane. Similarly, the carboxylate group is slightly rotated relative to the Thz heterocycle plane about the C2−C3 single bond. Coordination polymer chains propagate along [1 −1 −1] and are surrounded by three pairs of equivalent chains at distances of approximately 4.9 Å, 6.0 Å, and 5.4 Å, as shown in Figure 2.

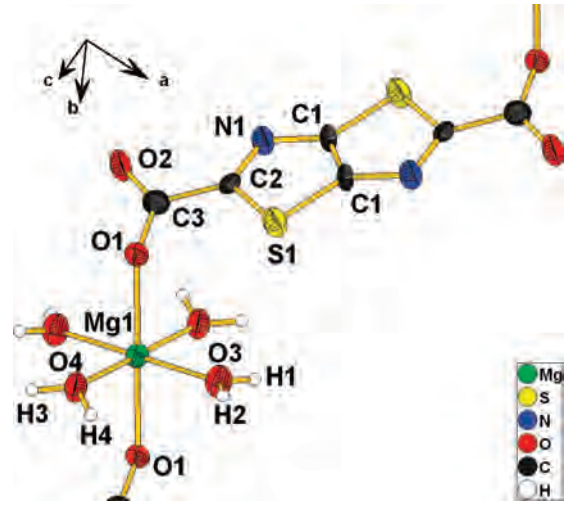

Figure 1. Thermal ellipsoid plot (50% probability) of **I**, with the atoms of one asymmetric unit (plus an extra O1 and C1) labeled. Both Mg1 and the Thz center sit on inversion centers. Hydrogen atoms are shown as white spheres.

$Ca_2(Thz)_2(H_2O)_8$, II. Similarly to **I**, compound **II** is a 1-D coordination polymer and crystallizes in the space group $P\bar{1}$. The connectivity of **II**, however, differs markedly from that of **I**: CaO_7 coordination polyhedra share an edge with one neighbor to form dimers around inversion centers (Figure 3). Two equivalent μ^2 water molecules (O5) bridge pairs of

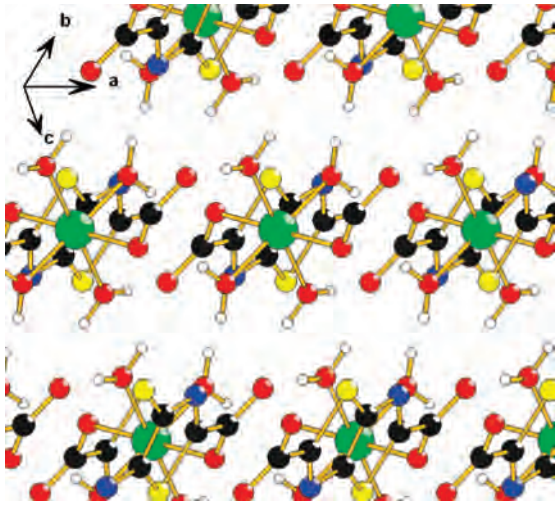

Figure 2. Chains of **I** viewed along the propagation direction [1 −1 −1]. Element colors are the same as in Figure 1.

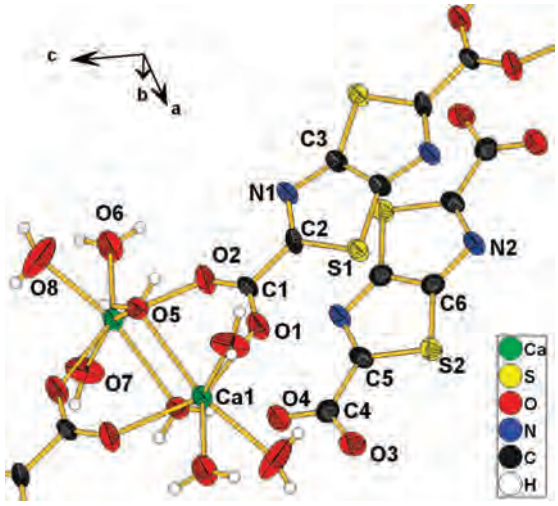

Figure 3. Thermal ellipsoid plot (50% probability) of **II**, with the atoms of one asymmetric unit labeled. Hydrogen atoms are shown as white spheres.

Ca^{2+} ions 3.82 Å apart to form a four-membered ring (and the shared edge of the polyhedra). Two opposite Thz carboxylate termini also bridge the Ca^{2+} ions, forming an eight-membered ring nearly perpendicular to the $Ca_2(\mu^2\text{-}H_2O)_2$ ring. Three terminal water molecules complete each Ca^{2+} coordination sphere to form pairs of distorted edge-sharing pentagonal bipyramids. The coordination polymer chains propagate through the Thz long axis, along [1 1 1]. The chain is positively charged, and uncoordinated Thz^{2-} anions provide charge balance. The anions lie between the 1-D chains, stacked between the bridging Thz units at a distance of ∼3.4 Å, as seen in Figure 4.

$Sr(Thz)(H_2O)_3$, III. Compound **III** crystallizes in the space group $P2_1/c$. Unlike **I** and **II**, it has extended inorganic connectivity in which SrO_7N polyhedra share edges to form an infinite chain (Figure 5). There is no connectivity between the chains. In contrast to **I** and **II**, only one carboxylate group of the Thz^{2-} ligand coordinates to the Sr^{2+} ions, through both oxygen atoms. O1 bridges two Sr^{2+} cations, while O2 bonds to a third one. Also unlike **I** and **II**, the nitrogen close to the bridging carboxylate (N1) bonds to the metal. An

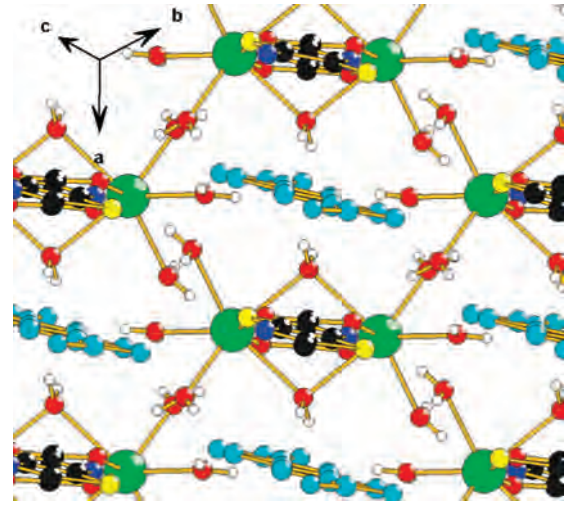

Figure 4. Chains of **II** viewed along the propagation direction [1 1 1]. Uncoordinated Thz^{2-} counterions occupy positions between chains. Except for the counterion Thz^{2-} in light-blue, element colors are the same as in Figure 3.

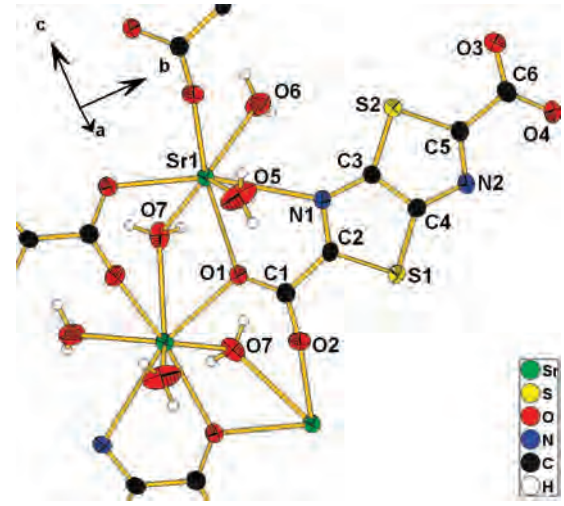

Figure 5. Thermal ellipsoid plot (50% probability) of **III**, with the atoms of one asymmetric unit labeled. Hydrogen atoms are shown as white spheres.

additional four oxygen atoms, two from equivalent bridging (μ^2) water molecules (O7) and two from coordinating water molecules (O5 and O6), complete the SrO_7N polyhedron. Edge-sharing takes place through O1 and O7, giving rise to 1-D M−O−M arrays along [0 0 1]. Figure 6 shows the relative chain arrangement in **III**. The chains are colored blue and red in order to differentiate their relative orientation.

Chains stack along the *a* direction, with consecutive stacks shifted (along *a*) by 1/2 of a cell. The chains' side groups interleave significantly, as seen in Figure 6a and b. The Thz heterocyclic rings stack parallel to each other and nearly overlap, displaced by about 1 Å toward their respective chain cores. The approximate stacking distance between the rings is 3.4 Å. Inversion centers between the stacks cause chains from consecutive stacks to propagate along opposite directions, rotated 180° about the propagation axis, as seen in Figure 6b. Each chain is surrounded by four such "inverted" chains, as seen in Figure 6a.

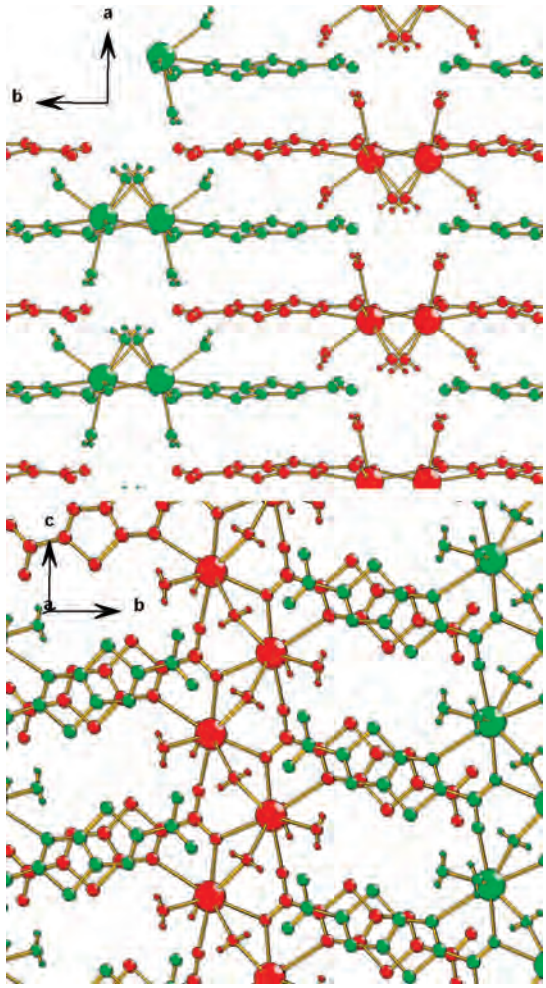

Figure 6. Packing of chains in **III**, shown along [0 0 1] (a) and [1 0 0] (b). Red and green chains are related by inversion symmetry. Ligand side groups interdigitate with and nearly eclipse those of neighboring chains.

Ba(Thz)(H$_2$O)$_7$, IV. Precipitation or crystallization from dilute solutions of H_2Thz and Ba(CH$_3$CO$_2$)$_2$ affords **IV**, which crystallizes in the space group *C*2/*c*. Like **I**−**III**, **IV** can be made at 100 °C. Compound **IV** exhibits the most extensive water coordination, with relatively sparse Thz coordination. BaO$_9$N polyhedra share three faces to form 2-D layers lying in the (0 0 2) planes (Figure 7). Each of two equivalent shared faces consists of one oxygen atom (O1) from the Thz ligand and two μ^2 water molecules (O7 and O8). The third shared polyhedral face consists of three μ^2 water molecules. N1 occupies the tenth and only nonbridging coordination site. This nitrogen coordination parallels what is observed with **III**. The second carboxylate oxygen, O2, does not coordinate the metal, nor do any atoms from the opposite end of the Thz group.

Figure 8a shows one layer formed by the face-sharing Ba polyhedra, demonstrating the 2-D M−O−M connectivity. Topologically, the connectivity of the polyhedra resembles the arrangement of carbon atoms within a graphene sheet, though the hexagons are irregular, with local 3-fold symmetry axes running through the gaps in the sheets. Consecutive layers are related by inversion symmetry. A side view of the relative layer arrangement (along *b*) is shown in Figure 8b. The figure clearly demonstrates the interdigitation of the

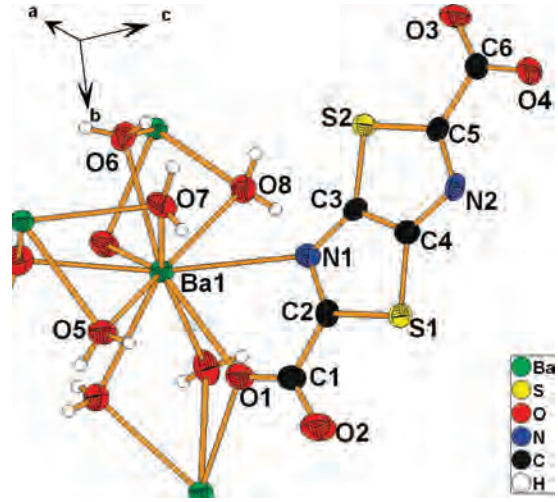

Figure 7. Thermal ellipsoid plot (50% probability) of **IV**, with the atoms of one asymmetric unit labeled. Hydrogen atoms are shown as white spheres.

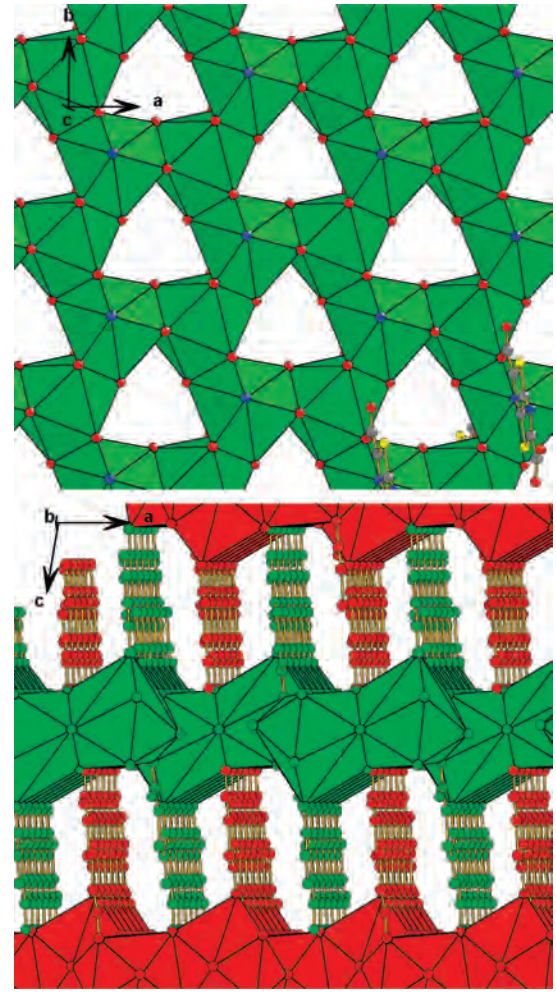

Figure 8. (a) Polyhedral representation of one layer of **IV** evidencing the 2-D M−O−M connectivity. Side groups omitted for clarity. (b) Side view of the relative layer arrangement in **IV**.

Thz termini toward adjacent layers. The free end of the ligand is directed at the trigonal gaps in the coordination layers above and below.

Thermal Behavior. Compounds **I**, **II**, and **III** all lose 16−18 wt % in the range 50−200 °C. For **I**, there seems to

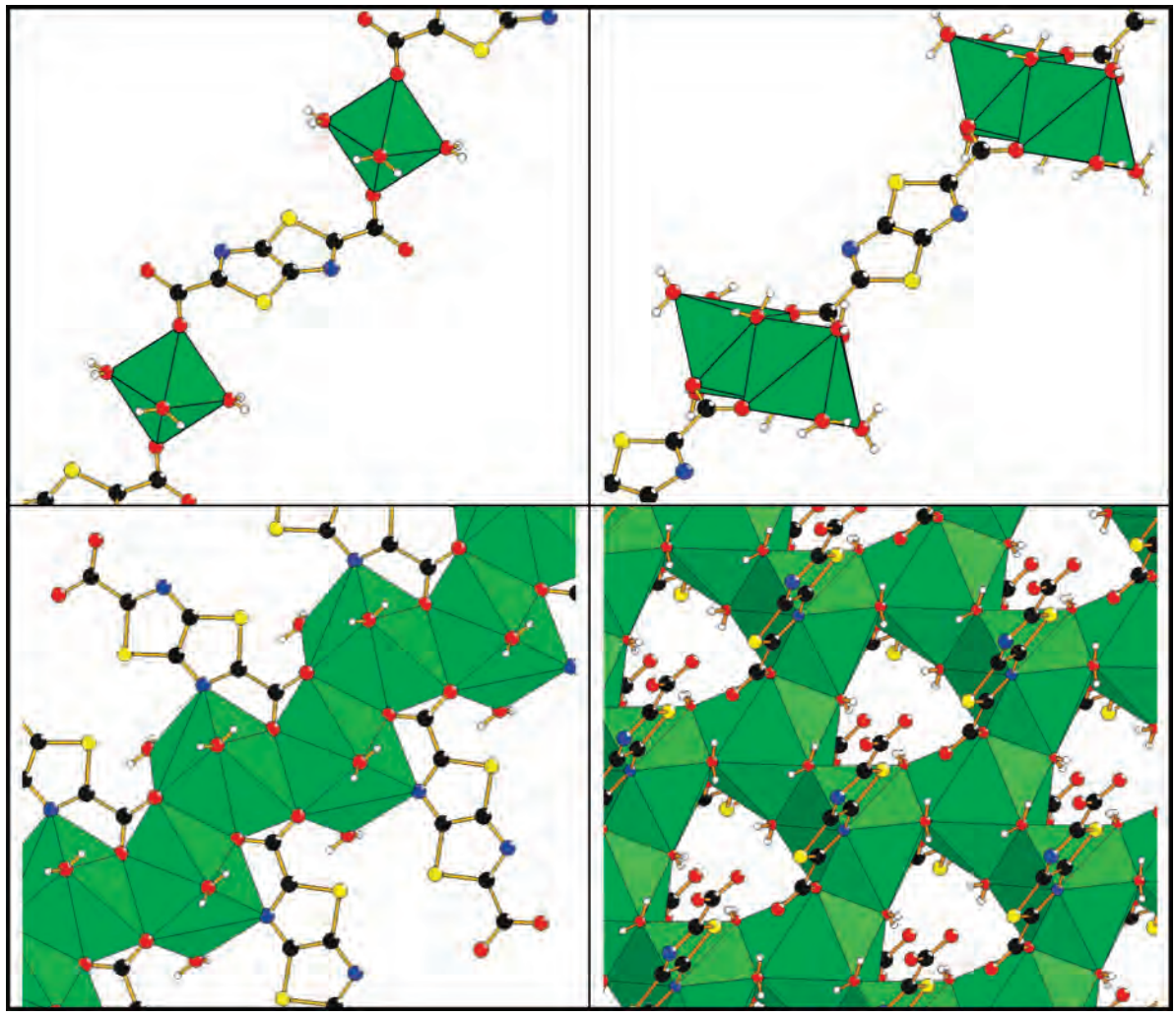

Figure 9. Structure comparison of compounds **I**−**IV**, polyhedral representation. M−O−M connectivity increases from isolated octahedra to dimers to chains to layers.

be an initial loss of two water molecules between 50 and 120 °C followed by the loss of a third one between 120 and 175 °C. Compound **II** behaves the same way, although the initial loss of the two water molecules seems to start even earlier. For **III**, there seems to be a loss of three water molecules up to ∼120 °C, with two additional small steps between 120 and 200 °C that might correspond to a fourth water molecule. For **IV**, a sharp weight loss amounting to ∼10.3 wt % takes place between ∼65 and 100 °C, followed by a slow loss of ∼2.9 wt % between 100 and 200 °C. These steps are likely due to the loss of five and one water molecule, respectively. All four compounds show a second, similar weight loss of 35−38% at higher temperatures. This is likely due to decomposition of the organic ligand. Compounds **I**−**III** again behave similarly, as this loss takes place within the broad range of 300−500 °C. A much sharper onset, starting at approximately 380 °C, is seen with **IV**, possibly due to a somewhat increased stability of the Ba-containing structure. Despite this, a variable-temperature XRD plot shows a loss of crystallinity for **IV** starting at 90 °C, probably caused by structure collapse upon water loss. The TGA profiles of compounds **I**−**IV** are presented in the Supporting Information.

Structural Trends. Figure 9 illustrates the M−O−M connectivity for compounds **I**−**IV**, showing the number of neighboring polyhedra connected to each other, as well as the dimensionality of the resulting M−O−M arrays. The inclusion of a thiazolo nitrogen atom in the metal coordination spheres of **III** and **IV** was decided on the basis of electrostatic bond valence calculations.[22−24] This nitrogen coordination arises not only from the increased coordination numbers of the larger cations but also because the nitrogen and its closest carboxylate oxygen are favorably situated to form a five-membered chelate ring with the larger cations. Both the cation coordination number and the number of connected neighboring polyhedra increase upon progressing from Mg to Ba, from 6 to 7 to 8 to 10 and from 0 to 1 to 2 to 3, respectively. In addition, the nature of the polyhedral connectivity changes from edge- to face-sharing in **IV**. In **I**, isolated Mg octahedra are connected through the ligand termini, while chains of dimeric Ca polyhedra occur in **II**; both compounds are classified as I^0O^1.[11] Edge-sharing Sr polyhedra form zigzag chains in **III**, and in **IV**, Ba polyhedra

(22) Brown, I. D. *Acta Crystallogr., Sect. B* **1977**, *33*, 1305.
(23) Brown, I. D.; Altermatt, D. *Acta Crystallogr., Sect. B* **1985**, *41*, 244.
(24) Brese, N. E.; O'Keeffe, M. *Acta Crystallogr., Sect. B* **1991**, *47*, 192.

share faces with three neighbors to form 2-D layers. Compounds **III** and **IV** are thus classified as I^1O^0 and I^2O^0, respectively.

Because the stoichiometry of these phases varies only slightly, the condensation of the metal polyhedra stems directly from the increase in the preferred coordination number of the metal cation. Specifically, the M−O−M connectivity varies as a result of the cation size and coordination number requirements. In addition, the current study has shown the ability of water itself to increase the inorganic connectivity within a framework structure, rather than limiting it, as is often the case with the transition metals.[12] Our results contrast with those of Côté and Shimizu[20] in the way that the cation selection affects the connectivity. In the latter study, it was shown that the overall dimensionality of alkaline earth metal organosulfonate salts may be increased sequentially from 0-D to 3-D upon progressing from Mg to Ba, as a direct effect of cation size. However, the dimensionality increase results entirely from increased connectivity through the organic ligand, with only finite M−O−M connections occurring in the form of dimers in the Ba compound. The compounds thus progress from I^0O^0 to I^0O^1, I^0O^2, and I^0O^3. This is possibly due to a lower ligand pK_a and a lower charge per oxygen in organosulfonates, as well as a more uniform distribution of coordinating groups in the ligand used in that work. The cation coordination numbers are 6 for Mg, 8 for Ca, and 9 for Sr and Ba.

In the present case, the limitations imposed by the ligand Thz^{2-}, the presence of bridging water molecules, and the increasing cation size (and thus coordination numbers) lead to the observed trends. The metal polyhedra behave as expected, with increasing coordination numbers.

Conclusions

We report the synthesis and structures of a series of alkaline earth hybrid frameworks in which the degree of inorganic connectivity varies directly with cation size (I^0O^1 to I^0O^1 to I^1O^0 to I^2O^0). Progression down the group also leads to an increase in the number of fused polyhedral neighbors (0 to 1 to 2 to 3, the latter through face-sharing), in the metal coordination number, and in the tendency for water molecules to bridge metal centers.

The large radii of the heavier alkaline earths allow water molecules to play the role of a bridging ligand rather than a capping ligand, thus increasing inorganic connectivity rather than limiting it, as is more often the case with other metals. In addition, the sizes of Sr and Ba allow the heterocyclic nitrogen atoms, together with carboxylate oxygen atoms, to coordinate the metal in a chelating mode. To the best of our knowledge, such a clear dependence of the inorganic connectivity solely upon cation size has not been reported among hybrid frameworks. It is hoped that the trends observed in this work will improve predictability in the synthesis of hybrid framework materials.

Acknowledgment. Financial support from the Department of Energy (Grant No. DE-FG02-04ER46176) and the use of the Materials Research Laboratory facilities are gratefully acknowledged.

Supporting Information Available: CIF files and a detailed procedure for the synthesis of 2,5-thiazolo[5,4-*d*]thiazoledicarboxylic acid (H_2Thz); details of single-crystal XRD data acquisition and refinement; complete lists of bond distances and angles; comparison between experimental and simulated powder XRD patterns; thermogravimetric analysis results; description of hydrogen-bonding schemes. This material is available free of charge via the Internet at http://pubs.acs.org.

IC8009173